

Effects of forest tent caterpillar defoliation on carbon and water fluxes in a boreal aspen stand

Jilmarie J. Stephens^{a,*}, T. Andrew Black^a, Rachhpal S. Jassal^a, Zoran Nesic^a, Nicholas J. Grant^a, Alan G. Barr^{b,i}, Warren D. Helgason^c, Andrew D. Richardson^{d,e}, Mark S. Johnson^f, Andreas Christen^{g,h}

^a University of British Columbia, Biometeorology and Soil Physics Group, Vancouver, British Columbia, Canada

^b Climate Research Division, Environment and Climate Change Canada, Saskatoon, Saskatchewan, Canada

^c University of Saskatchewan, Chemical and Biological Engineering, Saskatoon, Saskatchewan, Canada

^d Northern Arizona University, School of Informatics, Computing and Cyber Systems, Flagstaff, AZ, United States

^e Northern Arizona University, Center for Ecosystem Science and Society, Flagstaff, AZ, United States

^f University of British Columbia, Institute for Resources, Environment and Sustainability, Vancouver, British Columbia, Canada

^g Environmental Meteorology, Faculty of Environment and Natural Resources, University of Freiburg, Germany

^h University of British Columbia, Department of Geography/Atmospheric Science Program, Vancouver, British Columbia, Canada

ⁱ University of Saskatchewan, Global Water Institute for Water Security, Saskatoon Saskatchewan, Canada

ARTICLE INFO

Keywords:

Forest tent caterpillar
Eddy covariance
Gross ecosystem production
Ecosystem respiration
Net ecosystem production
Evapotranspiration

ABSTRACT

Insect outbreaks can significantly influence carbon (C) and water balances of forests. Forest tent caterpillars (FTC) (*Malacosoma disstria* Hübner) are one of the most prominent insects found in aspen forests in Canada and have the potential to considerably influence regional C and water fluxes. In the summer of 2016, an FTC infestation occurred in a ca. 100-year-old trembling aspen (*Populus tremuloides*) stand in the southern boreal forest where the long-term research site known as Old Aspen (OA) is located. The infestation led to nearly complete defoliation of the canopy during the leafing out period when photosynthesis, and thus C uptake, is progressing towards maximum levels. We used 21 years of eddy-covariance (EC) and climate measurements covering pre-infestation and infestation periods to estimate the impact of the FTC infestation on net ecosystem production (NEP), gross ecosystem production (GEP) and evapotranspiration (E). Defoliation in 2016 reduced annual NEP to $-130 \text{ g C m}^{-2} \text{ y}^{-1}$ and GEP to $798 \text{ g C m}^{-2} \text{ y}^{-1}$, respectively, which were much less than their 20-year means ($\text{NEP} = 118 \pm 53 \text{ g C m}^{-2} \text{ y}^{-1}$, $\text{GEP} = 1057 \pm 74 \text{ g C m}^{-2} \text{ y}^{-1}$), and resulted in the most negative annual NEP value of the 21 years of measurements at the OA site. NEP for 2016 was even lower than values observed during three drought years (2001–2003). However, FTC infestation caused little effect on annual E. FTC infestation reduced the near-surface remotely-measured greenness index, green chromatic coordinate (GCC), to ~ 0.32 on June 10 in comparison to ~ 0.40 in other years. The defoliation, observable from space as reductions in normalized difference vegetation index (NDVI) values, also showed a negligible effect on E but a large effect on the C fluxes.

1. Introduction

Nearly a tenth of all present-day global forest cover exists within Canada, which extends across 38% of the country's 9.1 million km² land area (FAO, 2015). Ecosystem disturbances such as wildfires, harvesting, insect outbreaks, and storms can have large effects on the carbon (C) balance of these forests (Amiro et al., 2010). Impacts of insect outbreaks on C balance tend to vary greatly depending on the species of insects and their host vegetation. Two types of insects that are known to

significantly alter C balance of a forest stand are: (1) *Coleoptera* (bark beetles) and (2) *Lepidoptera* (moths and butterflies) (Hicke et al., 2012; Peterson and Peterson, 1992). The latter, which are defoliators (also known as folivores), feed directly on tree leaves, thereby reducing the leaf area and affecting tree growth and mortality (Cook et al., 2008; Hogg et al., 2008). Such insect herbivores are often host-specific at the level of tree genus. In aspen stands (*Populus* spp.), the primary species of *Lepidoptera* capable of defoliation are the forest tent caterpillar (FTC) (*Malacosoma disstria* Hübner), large aspen tortrix (*Choristoneura*

* Corresponding author at: 136-2357 Main Mall, Vancouver, BC, V6T 1Z4, Canada.
E-mail address: jjstephe@mail.ubc.ca (J.J. Stephens).

conflictana), Bruce spanworm (*Operophtera bruceata*), aspen leaf miner (*Phyllocnistis populiella*), and gypsy moth (*Lymantria dispar*) (Peterson and Peterson 1992). The FTC in particular has been characterized as the most consequential insect of trembling aspen in the prairie provinces (Brandt, 1995), with several major outbreaks in the Canadian prairie provinces occurring between 1937 and 1990 (Brandt et al., 2003). FTC outbreaks tend to be periodic (separated by intervals of 9–13 years) and short-lived, lasting no longer than 1–2 years, though small areas of residual infestation can linger 4 years or longer (Cooke et al., 2009; Cooke and Lorenzetti, 2006). Despite the widespread, and sometimes severe, defoliation events caused by FTC, outbreaks rarely result in tree mortality on their own (Volney and Fleming, 2000), with the exception of outbreaks in locations where unusually frequent, long-lasting defoliation has occurred (Man and Rice, 2010). When FTC defoliation coincides with or immediately follows drought, increases in tree mortality have been observed (Hogg et al., 2008).

The life cycle of FTC has been previously described by Ives and Wong (1988), but we provide a brief summary here. Larvae hatch early in spring, which coincides temporally with the flushing of aspen leaves. Larvae do not actually produce a silken “tent”, but instead leave trails of silk while traveling to feed and rest in small silken masses spun on tree trunks or larger branches. After approximately 5 weeks, mature larvae form silken cocoons and pupate for about 10 days before emerging as moths. They then go on to lay eggs, which become larvae 4 weeks later but do not hatch until the following spring.

The impact of transient defoliation by insect herbivory on short-term fluxes has been the focus of some recent studies (e.g., Clark et al., 2010; Cook et al., 2008; Schäfer et al., 2010). Here, we examine an FTC infestation in 2016 that occurred at the boreal Old Aspen (OA) flux tower site in Saskatchewan (AmeriFlux ID “CA-Oas”) for the first time in the 21-year period of long-term flux monitoring at this site. The infestation led to a complete defoliation of the stand as shown in Fig. 1. Motivated by the unique opportunity afforded by a FTC defoliation event occurring in an intensively-instrumented forest stand, we have examined the impacts of this transient disturbance on seasonal and annual C and water fluxes. Quantification of the impact of FTC on C and water fluxes in 2016, compared to pre-disturbance measurements from 1996 to 2015, required the separation of the FTC impact from climate effects during 2016. This was achieved by simulating the fluxes for the FTC-infestation period assuming there was no infestation, and determining the impact by subtracting the measured fluxes.

2. Materials and methods

2.1. Site description

The OA study site is a mature deciduous broadleaf forest located near the southern edge of the boreal forest in Prince Albert National Park, Saskatchewan, in the Boreal Plains ecozone (53.62889°N, 106.19779°W, WGS-84). The forest consists of trembling aspen (*Populus tremuloides* Michx.) with scattered (~10%) balsam poplar (*Populus*

balsamifera L.) overstory and a hazelnut (*Corylus cornuta* Marsh.) understory. The understory accounts for 50% of the total leaf area (Arain et al., 2002; Barr et al., 2004). The stand is a uniformly aged stand that regenerated after a natural fire in 1919. The canopy height in 2002 was 21 m (Barr et al., 2012) and currently has a stem density of 486 trees ha⁻¹ (personal communication: Jay Maillet 3 March 2017). The soil, an Orthic Gray Luvisol, has developed on clay-rich glacial till that occurs below an 8–10-cm thick LFH (litter-fermented-humic) layer and a 30-cm-thick silt loam layer (Barr et al., 2012). Mean (1960–2000) annual precipitation and air temperature from the closest long-term climate stations – Waskesiu Lake (53.55°N, 106.04°W, 532 m elevation) and Prince Albert Airport (53.13°N, 105.67°W, 428 m elevation) – are 422 mm and 0.6 °C, and 408 mm and 0.9 °C, respectively.

2.2. Climate measurements

A suite of climate variables were measured and reported as half-hourly average values. Air temperature was measured with temperature/humidity sensors (model HMP45C, Vaisala Oy, Finland), which were housed in aspirated radiation shields at a height of 37 m. Air temperature was also measured with a platinum resistance thermometer (PRT) and a 36-gauge chromel-constantan thermocouple (Omega Engineering Inc., Laval, Quebec), both housed in an aspirated radiation shield (model 076B, Met-One Instruments Inc., Grants Pass, OR) at 36 m. Precipitation was measured using both a tipping bucket rain gauge (model TR-525, Texas Electronics Inc., Dallas, TX, USA or model CS700, Campbell Scientific Inc. (CSI), Logan, UT, USA) and a weighing rain gauge (model 3000 with an Alter shield, Belfort Instruments, Baltimore, MD, USA) which were located at a height of ~2 m on a raised platform in the center of a natural clearing approximately 50 m northeast of the tower. Antifreeze was added in winter to prevent freezing and motor oil was added in summer to minimize evaporative losses from the weighing rain gauge. Shortwave and longwave radiation were measured at the 36-m (downwelling) and 30-m height (upwelling) with paired pyranometers (model CM11, Kipp & Zonen BV, Delft, The Netherlands) and paired pyrgeometers (model PIR, Eppley Laboratory Inc., Newport, RI, USA), respectively. Upwelling and downwelling components of photosynthetically active radiation (PAR) were measured at the same heights with paired quantum sensors (model LI-190SA, LI-COR Inc., Lincoln, NE). About 95% of the down-facing radiometers’ canopy view would be within 43 m of the tower (Reifsnyder, 1967). Two profiles of soil temperature were measured at six depths (2, 5, 10, 20, 50, and 100 cm) with copper-constantan thermocouples.

2.3. Eddy-covariance flux measurements

We made year-round eddy-covariance (EC) measurements of fluxes of CO₂, water vapor, and sensible heat. These fluxes were measured using instruments mounted on a scaffold tower 39 m above the ground, including a tri-axial sonic anemometer (model R2 (1996–1999) or R3



Fig. 1. Photos of the forest tent caterpillar (FTC) defoliation event at the Old Aspen (OA) Fluxnet site taken on 16 June 2016 from the top of the tower within (a) and above the canopy (b). Panel (a) shows the branches stripped to the petioles with the FTC silken webs. In panel (b), the defoliated stand (over and understory) allows the green shrubbery on the forest floor to be seen.

(1999– present) Gill Instruments Ltd., Lymington, UK) and a closed-path, temperature-controlled infrared gas ($\text{CO}_2/\text{H}_2\text{O}$) analyzer (model LI-6262 or LI-7000, LI-COR Inc.). Air was drawn through a heated sampling tube (4 m length; 4 mm inner diameter Synflex 1300 tube (Saint-Gobain, Performance Plastics, Wayne, NJ)) by a diaphragm pump (model DOA-V191-AA, Gast Inc., Dayton, OH) at a flow rate of 10 L min^{-1} for the LI-6262 and 15 L min^{-1} for the LI-7000 (Krishnan et al., 2006; Barr et al., 2007, 2012). Daily automatic calibrations to correct CO_2 concentration measurements for zero and span shifts were implemented using CO_2 standard gases from the Greenhouse Gases Measurement Laboratory (GGML) of Environment and Climate Change Canada in Downsview, ON, Canada (Krishnan et al., 2006). The heated sample tube was replaced every 6 months to improve response times in H_2O and CO_2 sampling that are reduced due to dust, pollen, smoke particles or condensation in the tube. Half-hourly CO_2 , water vapour, sensible heat, and turbulent fluxes were calculated from the covariance of fluctuations in the vertical wind component and the scalar quantity of interest (i.e., mole mixing ratios of CO_2 or water vapour, and air temperature (Webb et al., 1980)) measured at 20 Hz and computed directly on the computer located at the site. Further details on the experimental setup, calibrations, calculations of fluxes and flux footprint analysis can be found in Griffis et al. (2003), Barr et al. (2004), Krishnan et al. (2006), Zha et al. (2010) and Chen et al. (2012).

2.4. PhenoCam observations

The PhenoCam Network (<http://phenocam.sr.unh.edu>) is a continental-scale network that provides automated, high-frequency near-surface remote sensing of canopy phenology. A PhenoCam is a high-resolution digital camera that takes photos every half hour and uploads them to the PhenoCam server, where images and derived data are made publicly available in near-real time. A PhenoCam has been monitoring canopy phenology at OA since 2011. The camera has a 1/2.5" CMOS imaging sensor, with a standard Bayer filter and is mounted at a height of approximately 32 m with a tilt angle, looking north such that the camera views about 20% sky, 80% canopy over an area of approximately 720 m^2 . There have been two cameras mounted on the tower, PhenoCam1 from 2011 to 2016 and PhenoCam2 from June 2016 to present. PhenoCam1 had a 4–10 mm zoom lens with a field of view of approximately 105° , while PhenoCam2 has a fixed 6.2 mm lens with a field of view of approximately 80° . Images are recorded at 1296×960 pixel resolution, as standard 3-layer red-green-blue (RGB) JPEG files with 8 bits per channel. Image processing consists of extracting RGB color channel information from the digital images, using methods described previously (Richardson et al., 2007; Sonnentag et al., 2012). “Chromatic coordinates”, indicating the relative intensity (pixel value, a digital number) of one channel against the overall intensity of all three channels together, termed as green chromatic coordinate (G_{CC}) can be readily calculated as $G_{CC} = G_{DN}/[R_{DN} + G_{DN} + B_{DN}]$, where G_{DN} , R_{DN} and B_{DN} represent the green (G), red (R), and blue (B) digital numbers, respectively. G_{CC} , widely-used in the phenological literature, is the product of the amount of foliage present and the color of individual leaves (Keenan et al., 2014). In a deciduous forest such as ours, increasing canopy greenness in spring is driven by the unfolding and expansion of new foliage, and consequently an increase in photosynthetic activity. Previous studies have linked canopy greenness indices (e.g., G_{CC}) to seasonal changes in net ecosystem C exchange and canopy photosynthesis (Richardson et al., 2007, 2009; Toomey et al., 2015). While G_{CC} tends to saturate at modest values of leaf area index (Keenan et al., 2014), the index has been successfully used to track canopy damage in response to extreme disturbance (Hufkens et al., 2012).

2.5. Normalized difference vegetation index (NDVI)

Daily normalized difference vegetation index (NDVI) values

corresponding to the OA tower location were obtained from the MODIS Terra platform for the 2001–2016 period using Google Earth Engine. Here, NDVI represents $(\text{NIR} - \text{Red})/(\text{NIR} + \text{Red})$ computed from the 7-band daily 500 m MOD09GA MODIS surface reflectance product (Vermote et al., 2015), where the red (Red) band is Terra band 1 (620–670 nm) and the near infrared (NIR) band is Terra band 2 (841–876 nm). Daily NDVI data were processed using the phenex package (Lange and Doktor, 2017) in R version 3.4.1 (R Core Team, 2017). This consisted of correcting and modeling the raw data using an asymmetric Gaussian function applied individually to each year to derive the long-term mean and standard deviation for each day of year for the 2001–2016 period. The corrected data for 2016 are presented with the long-term data set, also using the asymmetric Gaussian correction that has been shown to be the most effective for reducing noise in MODIS NDVI data for the boreal forest region (Hird and McDermid, 2009).

2.6. Data processing and quality control

Measurements and calibrations were checked daily (as part of a quality control/assurance routine) using a Matlab (Version 7.5, The Mathworks, Natick, MA, USA) program. Raw data went through three stages of cleaning before being used in calculations. In the first stage, data values with faulty measurements were removed but not replaced or interpolated. In the second stage, faulty measurements from specific sensors were replaced with the best available alternative measurements from redundant on-site instruments. Finally, in the third stage, temporal interpolation and gap filling based on diurnal variations was performed. All data cleaning procedures directly follow those described in Krishnan et al. (2006).

In the third data cleaning stage, net ecosystem production (NEP), gross ecosystem production (GEP) and ecosystem respiration (R_e) were calculated. NEP was determined using $\text{NEP} = -\text{NEE}$, where NEE is the net ecosystem exchange of CO_2 obtained directly from measurements of surface CO_2 flux corrected for the rate of change in air column CO_2 storage (we ignore negligibly small losses of dissolved organic C at the site). NEP is defined as the difference between C gained by GEP and C losses as a result of R_e . By this convention, NEP is positive for a C sink and negative for a C source.

We followed the Fluxnet-Canada Research Network (FCRN) procedure to estimate annual NEP, GEP and R_e as described in Barr et al. (2004) which is summarized below. R_e was estimated from NEP when GEP was known to be zero (nighttime and during the cold-season when both air (T_a) and soil (T_s) temperatures were $< 0^\circ\text{C}$). An empirical annual relationship between half hourly R_e and half hourly near-surface (2-cm) T_s for a friction velocity (u_*) $< u_*$ threshold of 0.35 m s^{-1} (Barr et al., 2004) was used to fill nighttime gaps and to estimate daytime R_e . GEP was estimated as $\text{NEP} + R_e$ (daytime) or zero (nighttime and during the cold-season, and gaps were filled using the rectangular hyperbolic relationship of GEP to PAR (i.e., the Michaelis-Menten light response equation). Gaps in NEP were then filled with the difference between the estimated GEP and R_e . To account for changes in other environmental variables such as soil moisture or vapor pressure deficit (D), a time-varying parameter was developed for each empirical relationship using a moving temporal window (Barr et al., 2004). This parameter is defined as the slope of the linear regression between estimated and measured values of R_e and GEP.

Uncertainty in annual NEP was quantified using three steps: (1) random error from each half-hour flux was estimated by adding a 20% random error per half hour as described in Morgenstern et al. (2004); (2) gap-filling procedure uncertainty was assessed by removing up to 40% of the data annually using a uniformly discrete random number generator, with 500 randomly selected continuous gap lengths ranging from a single missing half hour period to 10 days of data (480 half-hourly periods); (3) systematic bias due to the variation of the chosen u_* threshold was estimated by varying it by $\pm 20\%$ of our chosen

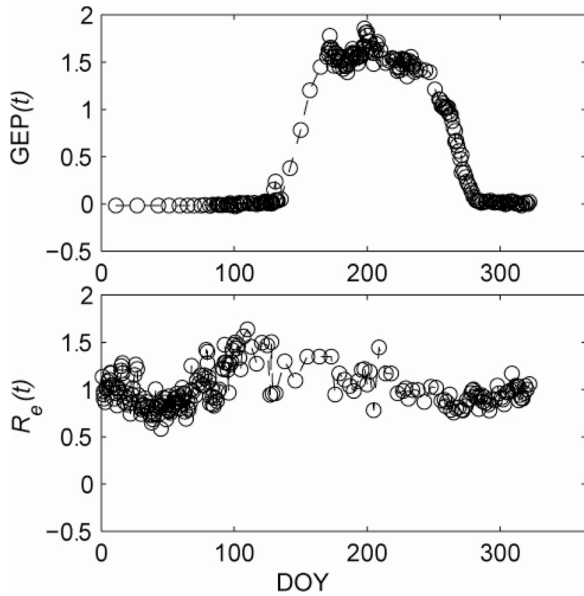


Fig. 2. Average values of the two time-varying parameters, $R_e(t)$ and $GEP(t)$ vs. day of year (DOY). Each value is the average of 4 values for the 4 years (1998, 2001, 2006, and 2010).

0.35 m s^{-1} threshold and then recalculating NEP. Total random error by taking the sum of squares of error from steps 1 and 2 was $\pm 17 \text{ g C m}^{-2} \text{ y}^{-1}$. The systematic error from step 3 was $\pm 36 \text{ g C m}^{-2} \text{ y}^{-1}$. Since the systematic error from choosing u_* will have a similar magnitude and direction each year, it is not random, and thus was added directly to the random error rather than using the sum-of-squares. The overall estimated uncertainty of annual NEP was $\pm 53 \text{ g C m}^{-2} \text{ y}^{-1}$. These values are comparable to those reported by Krishnan et al. (2006) using 11 years of data at this site. The same procedure was followed to calculate the uncertainty in annual GEP and R_e . The total random error from steps 1 and 2 was $\pm 21 \text{ g C m}^{-2} \text{ y}^{-1}$ and $\pm 20 \text{ g C m}^{-2} \text{ y}^{-1}$ for GEP and R_e , respectively. The systematic error from step 3 was $\pm 53 \text{ g C m}^{-2} \text{ y}^{-1}$ for GEP and $\pm 89 \text{ g C m}^{-2} \text{ y}^{-1}$ for R_e . The overall estimated uncertainty of annual GEP was $\pm 74 \text{ g C m}^{-2} \text{ y}^{-1}$ and for R_e was $\pm 109 \text{ g C m}^{-2} \text{ y}^{-1}$.

The same procedure as for the C fluxes was followed to estimate the uncertainty in annual E . The gap filling in step 2 for E relied on estimates of sensible and latent heat using a moving window based on Amiro et al. (2006). The total random error by taking the sum of squares of error from steps 1 and 2 was $\pm 7 \text{ mm year}^{-1}$. The systematic error from step 3 was $\pm 2 \text{ mm year}^{-1}$. The sum of these two errors produced an overall estimated uncertainty in annual E of $\pm 9 \text{ mm year}^{-1}$.

2.7. Estimating the impact of the FTC infestation on carbon and water fluxes

Data from four years (1998, 2001, 2006, and 2010) with early growing season onset within a week of the 2016 onset date (DOY 126) were chosen to parameterize the simulation of C and water fluxes in 2016 assuming there was no FTC infestation (see below). Growing season onset was defined as the calendar day when the daily average GEP made a significant jump (from $< 0.8 \mu\text{mol m}^{-2} \text{ s}^{-1}$ winter levels to $> 1 \mu\text{mol m}^{-2} \text{ s}^{-1}$) and was followed by a rapid increase thereafter. For the four years (1998, 2001, 2006, 2010), the onset dates were DOY 123, 125, 127, 133 with three of the years having growing season onsets within ± 3 days of that for 2016. The growing season onset was checked by calculating cumulative growing-season degree days following the method of Barr et al. (2004). Using the day of the year when 100 ° days were reached to define the start of the growing season, it also

occurred on DOY 126 in 2016. Following this method for the four years, the growing season onset dates were DOY 123, 132, 120, 134 (in close agreement with the observed onset dates listed above) are within ± 8 days of that for 2016.

To calculate what the 2016 C fluxes would have been in the absence of an FTC outbreak, we used the same physiological equations to estimate R_e and GEP as in the FCRN gap filling procedure (Barr et al., 2004). We applied the procedure to the complete gap-filled record from each of the four years listed above to retrieve parameters for the empirical relationships and the time varying parameters in Eqs. (1) and (2) below to calculate half-hourly values of R_e and GEP in $\mu\text{mol m}^{-2} \text{ s}^{-1}$ for 2016 using, respectively:

$$R_e = R_e(t) \frac{b_1}{1 + \exp^{b_2(b_3 - T_s)}} \quad (1)$$

where $R_e(t)$ is the time variation in R_e (see below) which accounted for the seasonal variations in other climate variables (e.g., soil moisture), T_s is the half-hourly value of 2-cm soil temperature ($^{\circ}\text{C}$) and b_1 ($\mu\text{mol CO}_2 \text{ m}^{-2} \text{ s}^{-1}$), b_2 ($^{\circ}\text{C}^{-1}$) and b_3 ($^{\circ}\text{C}$) are fitted parameters (Table A1); and

$$GEP = GEP(t) \frac{c_1 Q}{c_2 + Q} \quad (2)$$

where $GEP(t)$ is the time variation in GEP (see below) which accounted for the seasonal variations in other climate variables, Q is half-hourly downwelling PAR ($\mu\text{mol photons m}^{-2} \text{ s}^{-1}$) for 2016, and c_1 ($\mu\text{mol CO}_2 \text{ m}^{-2} \text{ s}^{-1}$) and c_2 ($\mu\text{mol photons m}^{-2} \text{ s}^{-1}$) are fitted parameters that vary with light (Table A1). We found that the model performed better when applied separately for low light (PAR $< 800 \mu\text{mol photons m}^{-2} \text{ s}^{-1}$) and high light (PAR $> 800 \mu\text{mol photons m}^{-2} \text{ s}^{-1}$) conditions.

In the estimation of different parameters in Eqs. (1) and (2), first b_1 – b_3 and c_1 and c_2 were estimated achieving the best fit to measured R_e and GEP data, respectively. Then $R_e(t)$ and $GEP(t)$ were calculated as the ratios of the respective measured values to those estimated by using the fitted parameters (b_1 , b_2 , etc.) using a moving window. The optimal window size was found to be 100 data points (~ 2 days). Fig. 2 shows the average values of the two time-varying parameters obtained using the moving-window procedure. Then NEP was calculated from $\text{NEP} = \text{GEP} - R_e$. The simulation uncertainties associated with annual estimates of R_e and GEP were assessed by varying the simulation parameters (b_1 – b_3 and $R_e(t)$ for R_e and c_1 , c_2 for both light levels, and $GEP(t)$ for GEP by $\pm 10\%$ to simulate new half-hourly values and summed to provide new annual estimates.

To estimate the values of E that would have occurred without FTC infestation, we used the Priestley-Taylor approach (Priestley and Taylor, 1972). Daily average climate was used to calculate daily values of the Priestley-Taylor alpha (α) for each of the four years, which were averaged to obtain mean daily (24-h) α values, using

$$\alpha = \frac{\lambda E}{[s/(s + \gamma)] R_a} \quad (3)$$

where E is the daily (24 h) water vapor flux (evapotranspiration) ($\text{kg m}^{-2} \text{ day}^{-1}$ or mm d^{-1}), R_a is the available energy flux (W m^{-2}), which is given by ($R_a = R_n - G$) (neglecting energy storage change in the air column beneath the flux measurement sensors on the tower) where R_n is daily net radiation (W m^{-2}), G is daily soil heat flux (W m^{-2}), s is the slope of the saturation vapor pressure curve ($\text{kPa } ^{\circ}\text{C}^{-1}$), λ is the latent heat of vaporization (J kg^{-1}), and γ is the psychrometric constant ($\text{kPa } ^{\circ}\text{C}^{-1}$). The three latter variables were evaluated at half-hourly scales and then averaged to daily values. α values were calculated using two methods: using Eq. (3) and replacing $R_n - G$ with $H + \lambda E$ where H is the daily sensible heat flux and λE is the daily latent heat flux. The latter method was used by Krishnan et al. (2006) to avoid issues of energy-balance non-closure, since the substitution of $H + \lambda E$ has the same effect on α as adjusting $H + \lambda E$ to force

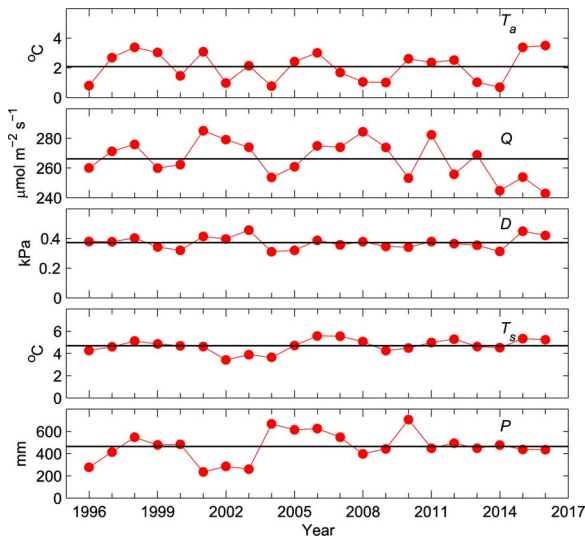


Fig. 3. Annual average 24-h averaged air temperature (T_a), downwelling photosynthetically active radiation (Q), vapor pressure deficit (D), 2-cm soil temperature (T_s) and annual precipitation (P) from 1996 to 2016 with the 21-year mean shown by the black line.

energy balance closure (Barr et al., 2002). The mean daily α values were then used to simulate E for 2016 as if there had been no FTC infestation, using

$$E = \alpha \left(\frac{sR_a}{s + \gamma} \right) \left(\frac{1}{\lambda} \right) \quad (4)$$

E was calculated using the same two methods used to calculate α . To account for the change in shortwave albedo (ρ_s) due to the defoliation, the average daily ρ_s values from the four years were used to estimate what daily R_n would have been during 2016 without defoliation. The simulation uncertainty in estimating annual E was determined by varying α by 10% and summing to retrieve new values.

3. Results

3.1. Climate measurements

Fig. 3 shows the interannual variation in the annual average T_a , PAR, D , and T_s . The values of several climate variables in 2016 exceeded ± 1 standard deviation relative to the long-term mean of the observed record at OA. 2015 and 2016 exhibited the highest annual T_a on record (3.49°C ($> +1\sigma$) in 2016 versus a long-term (1996–2015) mean of 2.28°C). Since 2008, there was a slightly decreasing trend in PAR, and the 2016 mean value was the lowest on record ($243 \mu\text{mol m}^{-2} \text{s}^{-1}$ ($< -1\sigma$) versus a long-term mean of $266 \mu\text{mol m}^{-2} \text{s}^{-1}$). The same trend, and the lowest value on record, was observed in the downwelling shortwave radiation. Mean value of D in 2016 was the third highest on record (0.42 kPa ($> +1\sigma$) in 2016 versus a long-term mean of 0.37 kPa). In 2016, the mean annual T_s of 5.23°C was among the 5 warmest years in terms of T_s at the 2-cm depth in the last 21 years. P over the 1996–2016 period of record exhibited high inter-annual variability (range 237–710 mm; standard deviation 128 mm), with the three drought years during 2001 to 2003 (Krishnan et al., 2006). Average annual P increased by 21.4% from 433 mm for the pre-drought years (1996–2000) to 538 mm in the post drought years (2004–2015) (Fig. 5b). This increase in annual P is consistent with the observed wetting of Northern Hemisphere mid-latitudes (30°N – 60°N) between 1901–2008 (Stocker et al., 2013). In 2016, P at OA (457 mm) was 10% lower than in the previous 4 years.

Fig. 4 shows how temporal variation in climate variables in 2016 compared with those for 1996–2015. T_a mostly followed the well-

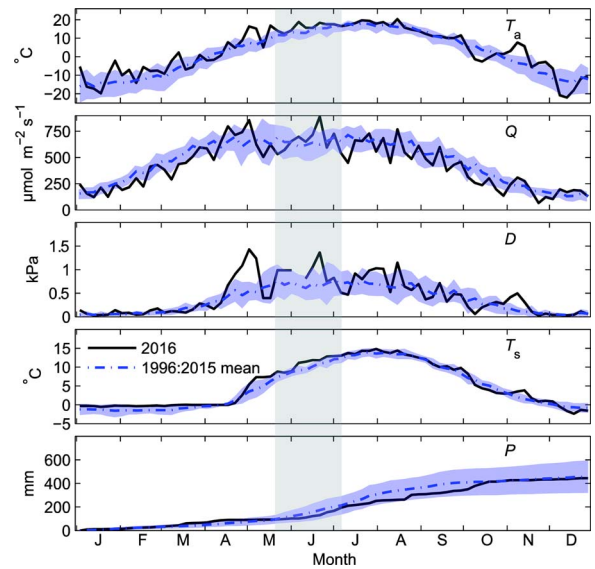


Fig. 4. Five-day averaged air temperature (T_a), photosynthetically active radiation (Q), vapour pressure deficit (D), 2-cm soil temperature (T_s) and cumulative precipitation (P) from 1996 to 2015 by the blue dot-dashed line and 2016 by the black line. Shaded blue areas denote $\pm 1\sigma$ from the mean. The grey bar indicates the duration of the defoliation event. (For interpretation of the references to colour in this figure legend, the reader is referred to the web version of this article.)

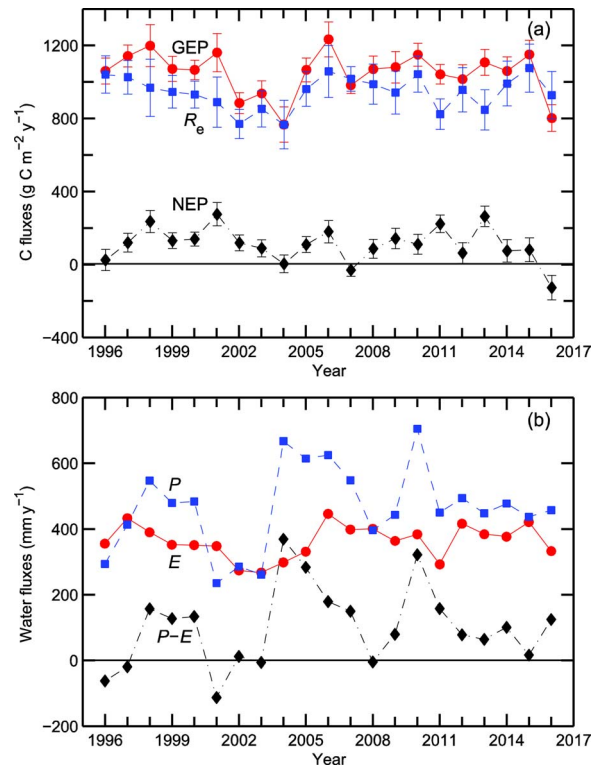


Fig. 5. 1996–2016 Annual values of (a) gross ecosystem production (GEP) (red circles), ecosystem respiration (R_e) (blue squares), net ecosystem production (NEP) (black diamonds) and (b) evapotranspiration (E) (red circles), precipitation (P) (blue squares) and precipitation excess ($P - E$) (black diamonds) with magnitudes of the uncertainty bars calculated as described in Section 2.6. Note that uncertainty bars are present in panel b, but are not visible because the magnitude of uncertainty spans a smaller range than the markers. (For interpretation of the references to colour in this figure legend, the reader is referred to the web version of this article.)

defined seasonal cycle observed in prior years, and was generally within one standard deviation of the long-term mean. However, there were several notable departures from the mean T_a during key time

periods—including one at the start of the growing season in late April, indicating a rapid spring warm up. PAR values in 2016 were below the average values for most of the year except for early April, which was likely related to the rapid warming at this time and the overall early start of the growing season. D generally tracked T_{as} , although in this case the April anomaly was even more pronounced.

Soil temperature at the 2-cm depth in 2016 was above the 20-year mean, with the initial spring warming spike in late April falling well outside one standard deviation from the mean. The 2016 winter and early spring were wetter than usual, but by April cumulative P plateaued, remaining depressed throughout the growing season and did not return to the long-term mean until mid-October yielding an annual total (457 mm) only slightly less than the 1996–2015 average value (465 mm).

3.2. Long-term carbon and water fluxes

For nearly all of the years in 1996–2015, prior to the FTC-induced defoliation event in 2016, OA had been a moderate C sink ($NEP = 118 \pm 53$ (mean \pm average uncertainty) $g C m^{-2} y^{-1}$ (Fig. 5a)), with mean GEP and R_e of $1058 \pm 74 g C m^{-2} y^{-1}$ and $941 \pm 109 g C m^{-2} y^{-1}$, respectively. The two exceptions were in 2004 and 2007. In 2004, following the three-year drought, near-zero NEP ($0 \pm 32 g C m^{-2} y^{-1}$) resulted from a cool spring and the combination of a large decrease ($296 g C m^{-2} y^{-1}$) in GEP and only a small decrease ($179 g C m^{-2} y^{-1}$) in R_e compared to the longterm means (Barr et al., 2007). In 2007 NEP was well below zero ($-34 \pm 25 g C m^{-2} y^{-1}$) with slightly below-average GEP ($978 \pm 46 g C m^{-2} y^{-1}$) but above-average R_e ($1013 \pm 67 g C m^{-2} y^{-1}$). In 2016, the NEP value ($-130 \pm 57 g C m^{-2} y^{-1}$) was far below the second lowest value of $-34 g C m^{-2} y^{-1}$ in 2007. The extremely low NEP value in 2016 resulted from the different responses of GEP and R_e to defoliation (Fig. 9). The value of GEP in 2016 ($798 \pm 73 g C m^{-2} y^{-1}$) was similar to the 2004 value, despite the near-total defoliation during mid-May to mid-June in 2016. The early spring rise in GEP in 2016, associated with a warm spring and early leafout, partly offset the reduction in GEP by defoliation. In contrast to the below-average GEP in 2016, R_e remained near normal ($928 \pm 129 g C m^{-2} y^{-1}$).

Interannual variation in annual E was, in general, closely linked to the variation in annual P (Fig. 5b), although somewhat subdued. While P in 2016 was 10% lower than the previous 4 years, 2016 E (332 mm) was well within the previously observed range and not nearly as low as observed during the 2001–2003 drought years. Furthermore, $P-E$ (precipitation excess) increased slightly in 2016 due to a small drop in E . Note that $P-E$ is a relative rather than an absolute index of water excess, because of the lack of closure in the surface energy balance; applying an energy-closure fraction of 0.88 to E (as reported by Barr et al. (2012) at this site) would increase E and reduce $P-E$ by $\sim 50 mm y^{-1}$.

3.3. Defoliation dynamics

The start of the 2016 growing season was among the earliest in our 21-year record (ranked = 4th by flux method or tied for 3rd using growing degree days). In May 2016, the FTC attack caused complete defoliation of the stand including the hazelunt understory (Fig. 1b) with subsequent recovery to near normal greenness near the end of the growing season. This progression of phenological changes was tracked by the PhenoCam, as shown in Fig. 6. Unfortunately due to malfunctioning of the PhenoCam, we do not have photographs, and therefore measured G_{CC} values, for the initial stage (29 April (DOY 120) to 13 May (DOY 134)) of the 2016 growing season and again later in the growing season from 2 June (DOY 154) to 16 June (DOY 168). For this reason we also present ρ_s and NDVI values, derived from MODIS, which are described below. We gap filled the measured G_{CC} values by fitting a cubic polynomial between G_{CC} and the ρ_s during the green-up period

(DOY 126–150) with R^2 of 0.88 and RMSE of 0.012. Between 2012 and 2015, G_{CC} before the start of canopy green-up had an average value of 0.310. In 2016, it was 0.313 on 29 April (DOY 120), but by 13 May (DOY 134), it had already increased to 0.371 (Fig. 7a). The gap-filled G_{CC} values reached a maximum of 0.387 on 15 May (DOY 136) which was 84% of the seasonal amplitude progressing to the average maximum G_{CC} (0.402). In comparison, the average value from the past four years (0.326) only reached 17% of the seasonal amplitude by 15 May (DOY 136). The difference between 2016 and the past four years (2012–2015) could be due to the uniquely early start of the growing season in 2016. During the defoliation event, G_{CC} dropped to a minimum value of 0.322 on 18 June (DOY 170) and subsequently started to recover. Upon stand refoliation, the maximum 2016 G_{CC} value was 0.387, which was $\sim 96\%$ of the average maximum G_{CC} (0.402), and occurred about a month later than is typical (Fig. 7a).

The seasonal progression of ρ_s from 2012 to 2016 showed the impact of an early growing season start and defoliation in 2016 on the stand's radiation dynamics (Fig. 7b). Change in ρ_s is highly correlated to that of G_{CC} , as expected from the high R^2 and low RMSE between the two variables during the green-up period, and shows the gap filling approach captured the timing and magnitude of change quite well. ρ_s does have a greater increase in magnitude past 16 May (DOY 137) compared to G_{CC} and reached a maximum value of 0.13 on 21 May (DOY 142) compared to the maximum G_{CC} on 15 May (DOY 136). The minimum ρ_s value of 0.097 occurred on 14 June (DOY 166) four days earlier than the minimum value recorded by the two PhenoCams. If either PhenoCam had been functional during that period then possibly the occurrence date of the minimum would be in agreement. ρ_s stopped increasing on July 2 (DOY 184) when it reached 0.128 falling directly in the middle of the spread of values in the previous four years on that date (0.122–0.141).

Daily NDVI values were aggregated into long-term means for each DOY in order to compare the 2016 infestation period to typical land surface phenology (Fig. 8.). The 2016 NDVI values exhibited an earlier than average increase in NDVI due to the early growing season start and an unusual decline within the growing season starting at DOY 140, as with G_{CC} and ρ_s , corresponding to the FTC infestation. The NDVI shows the effect of the defoliation but may blunt it due to coarse pixel resolution and by not covering the same flux footprint area as the tower. Chen et al. (2011) found 90% annual flux footprint from 1.2 km during 2006 at OA. Kljun et al. (2006) found that under convective conditions the 90% flux footprint was typically 450–550 m at OA, while during stable or neutral conditions it was typically 900 m. This research indicates that the MODIS NDVI pixel is only capturing a fraction of the flux footprint. Landsat8 NDVI was used to help quantify the extent of defoliation attack within the flux footprint using 3 dates (Fig. A1): 18 June 2015 (one year before the attack), 16 May 2016 (maximum greenup prior to attack, though not yet to anticipated peak greenness), and 17 June 2016 (date of maximal influence of attack on NDVI as determined from MODIS derived values, Fig. 8). The median NDVI values for the three dates were 0.79, 0.54 and 0.21, indicating that the defoliation event decreased the NDVI by 73% compared to nearly the same June day value in 2015. The majority of the Landsat data for the 2 km by 2 km area corresponding to the flux tower footprint has an NDVI less 0.3 by 17 June 2016, excluding two areas: one located north and another in the south to south-west. Landsat8 has a finer spatial resolution, 30 m by 30 m, but has a lower temporal resolution (8-day compared with the daily MODIS data), so it is useful to see the spatial heterogeneity of the attack, but not the temporal dynamics. Visual observations on site showed the defoliation to be most extreme at the tower site, tapering off from the tower (Fig. A2.).

3.4. Simulation validation

To evaluate the method used to estimate what the C fluxes would have been without defoliation, the method was applied to each of the

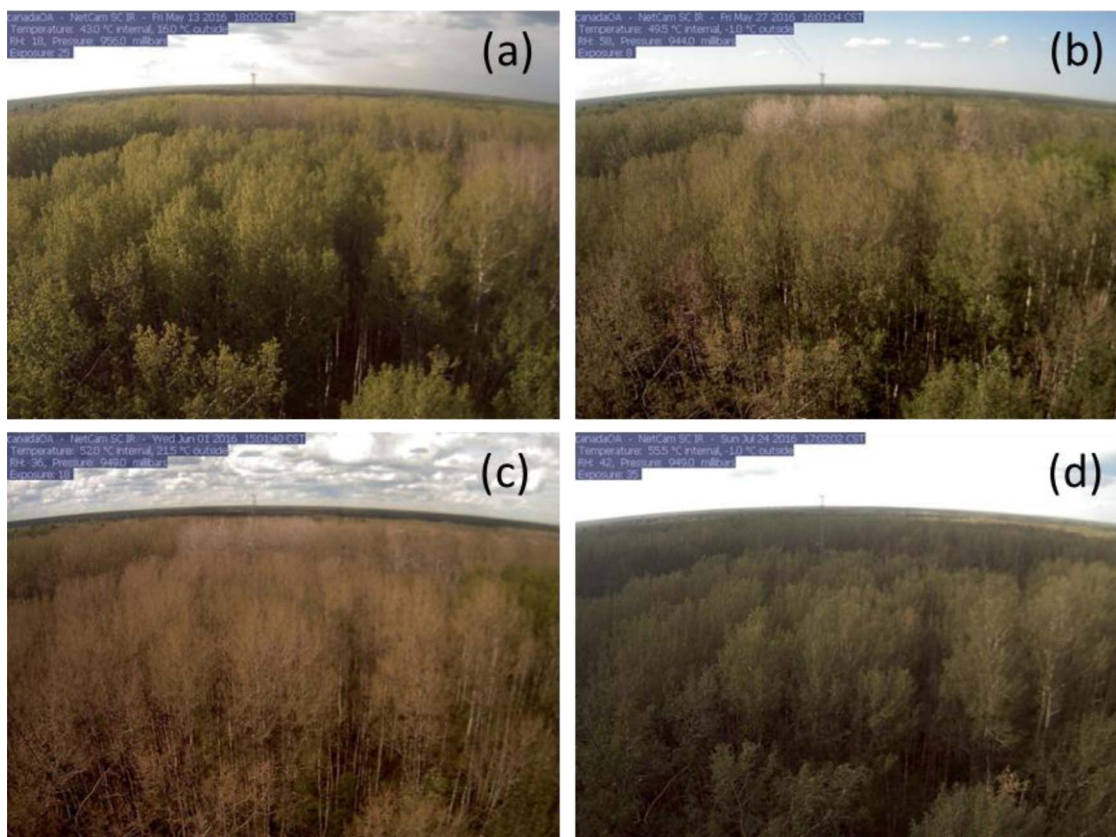


Fig. 6. PhenoCam photographs taken from the top of the flux tower on 13 May 18:00 CST (a), 27 May 16:00 CST (b), 1 June 15:00 CST (c), and 24 July 15:00 CST 2016 (d).

reference years (1998, 2001, 2006, and 2010). We compared simulated and observed C and water fluxes for the four years, both as a four-year average and for each year individually by using average climate and parameter values and individual-year values, respectively. For the individual-year simulations, the parameters used were the average of the three values from the three other years, to ensure independence. Results (Table A2) showed that daily average simulated GEP either over or underestimated (+11% to -1%) measured GEP for individual years. The simulated annual GEP for individual years deviated from the measured GEP by an average of $53 \text{ g C m}^{-2} \text{ y}^{-1}$ which falls within the average measurement uncertainty of $95 \text{ g C m}^{-2} \text{ y}^{-1}$ for those years. However, when parameter values averaged over the four years were used, the model yielded a slope of 1.00 between the measured and the modeled GEP values as shown in Fig. A3a. The simulated annual GEP from the average of the four years was only $10 \text{ g C m}^{-2} \text{ y}^{-1}$ less than the average of the measured GEP from the four years. Simulated R_e was either over or underestimated for individual years (+18% to -8%) with the average of the four years being overestimated by 9% and yielding a slope of 1.09 between the average of the measurements and the simulated results. R_e was systematically overestimated for years with larger (> 1500 °C days) cumulative growing degree days and underestimated for years with smaller cumulative growing degree days. The long-term mean cumulative growing degree day total was $1453 \pm 159 \text{ °C days}$. We attempted to improve the R_e simulation by stratifying on T_s similar to the method used for GEP, but the method did not work well. The lack of improvement in this method is likely due to heterotrophic respiration being more affected by soil moisture variation which is not accounted for here, compared to autotrophic respiration and GEP which have similar response to temperature variations. Thus, we found it necessary to correct the R_e simulation by multiplying simulated R_e output by the slope of the linear regression between the measured and simulated R_e , which resulted in a new slope of 1.03 (Fig. A3b). Consequently, the corrected simulated annual R_e from individual

years differed from measurements by an average of $32 \text{ g C m}^{-2} \text{ y}^{-1}$ while the average measurement uncertainty was $134 \text{ g C m}^{-2} \text{ y}^{-1}$. The simulated R_e from the average of the four years was $19 \text{ g C m}^{-2} \text{ y}^{-1}$ less than the average of the measured R_e for the four years.

The simulated annual values of GEP and R_e led to the calculated NEP for individual years deviating on average $52 \text{ g C m}^{-2} \text{ y}^{-1}$ from the measured value, which was within the $60 \text{ g C m}^{-2} \text{ y}^{-1}$ average measurement uncertainty for these years. The calculated NEP from the simulation ran on the average of the four years resulted in simulated NEP being $10 \text{ g C m}^{-2} \text{ y}^{-1}$ greater than the average measured NEP for the four years. For simulated E , the average Priestley-Taylor α during most of the growing season (June–Sept) was greater than 1 reaching a maximum of 1.18 (Fig. A3c). The small variation in α between years led to a slope of 0.99 in the linear regression (not shown) between simulated and measured E with an R^2 of 0.99.

3.5. Impact of FTC infestation on carbon and water fluxes

The 2016 growing season, delineated using daily GEP, began with a strong GEP of $2.3 \text{ g C m}^{-2} \text{ d}^{-1}$ (24-h average) on 6 May (Fig. 9a). Measured GEP continued to increase to $2.9 \text{ g C m}^{-2} \text{ d}^{-1}$ until 11 May but then dropped to $1.3 \text{ g C m}^{-2} \text{ d}^{-1}$ on 12 May and remained below $2 \text{ g C m}^{-2} \text{ d}^{-1}$ until 14 June as a result of canopy defoliation. On refoliation, GEP quickly increased once again, reaching $10.5 \text{ g C m}^{-2} \text{ d}^{-1}$ two and a half weeks later (2 July). Unlike the measured values, the simulated FTC-free GEP values continued to increase after 11 May, reaching a maximum value of $17.5 \text{ g C m}^{-2} \text{ d}^{-1}$ on 30 June and then declining to match the measured flux on 3 July. It either matched or was slightly lower than the measured values for the rest of the year. Our results show that the FTC attack depressed GEP for five weeks during the usually productive early portion of the growing season (Fig. 9a).

The difference between measured and simulated FTC-free R_e was significantly less than that for GEP (Fig. 9b). The two values began to

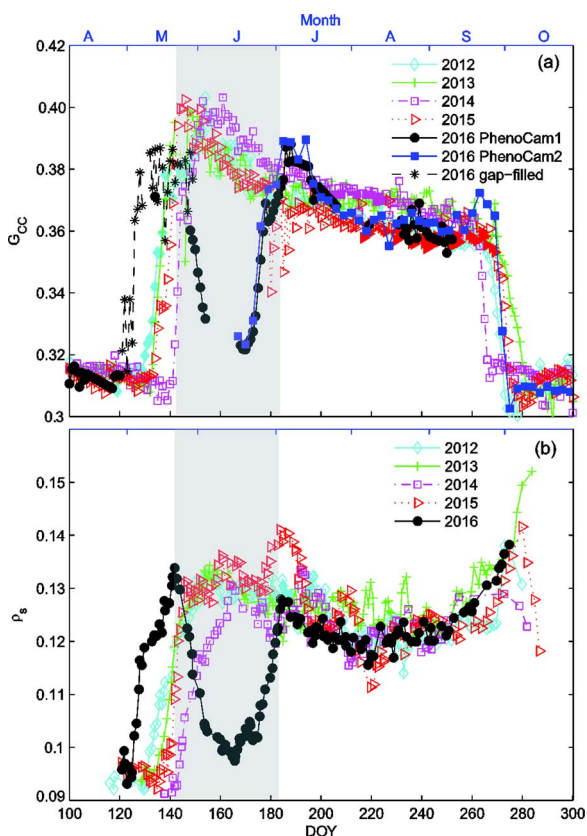


Fig. 7. Growing season progression of the green chromatic coordinate (G_{CC}) (a) and shortwave albedo (ρ_s) (b) for 2012–2016. PhenoCam1 was the camera that had been running since 2012 and PhenoCam2 was installed on 16 June 2016. The asterisk values are gap-filled by a cubic polynomial of the relationship between green-up G_{CC} values and shortwave albedo. The grey bar indicates the duration of the defoliation event. (For interpretation of the references to colour in this figure legend, the reader is referred to the web version of this article.)

diverge after 14 May, becoming considerably larger after 22 May when measured R_e began to decrease while simulated R_e continued to increase (Fig. 9b). After 11 July, measured R_e decreased while simulated R_e continued to increase. This difference was likely due to low P during July and August (Fig. 4). The two traces remained divergent until 15 August. Both measured and simulated NEP (Fig. 9c) were negative (as low as $-3.9 \text{ g C m}^{-2} \text{ d}^{-1}$ on 5 May) and remained comparable until 14 May when they diverged, with simulated NEP quickly becoming increasingly positive and measured NEP returning to negative values. Simulated NEP reached a maximum value of $10.7 \text{ g C m}^{-2} \text{ d}^{-1}$ on 23 June while measured NEP was negative ($-1.0 \text{ g C m}^{-2} \text{ d}^{-1}$) so that, like GEP, they did not match again until 3 July. Simulated NEP was less than measured NEP (Fig. 9c) because simulated R_e was much higher than measured R_e from 11 July to 10 August.

The impact of the defoliation on E was much subtler than on C fluxes (Fig. 9d). Starting on 3 May 2016, measured E was 0.93 mm d^{-1} increasing to 2.5 mm d^{-1} on 21 May and subsequently decreasing to less than 2 mm d^{-1} for the next 17 consecutive days. Then it slowly increased to its growing season maximum of 5.7 mm d^{-1} on 25 July and steadily decreased thereafter. Simulated E remained somewhat lower than measured E until 24 May, at which point simulated E increased to 1.5–2 times greater than measured E for a 4-week period (Fig. 9d).

These differences in the temporal progression of measured and simulated fluxes led to a significant difference in annual C fluxes, but not in annual E (Fig. 10). Measured GEP values during 2016 summed to $798 \pm 73 \text{ g C m}^{-2} \text{ y}^{-1}$, while simulated values assuming no FTC infestation summed to $1098 \pm 130 \text{ g C m}^{-2} \text{ y}^{-1}$. Thus, the FTC infestation

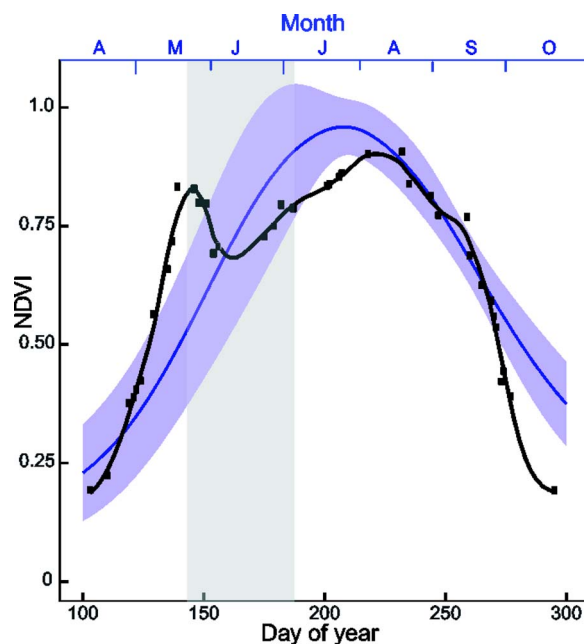


Fig. 8. NDVI values for a 500-m MODIS pixel representing the Old Aspen tower location. The black squares correspond to NDVI values for 2016, fit with a LOWESS smoothing function (black line). The blue line represents the mean NDVI values for each day of year over the 2001–2016 period with the shaded blue area corresponding to ± 1 standard deviation from the mean for each day of year. The grey bar indicates the duration of the defoliation event. (For interpretation of the references to colour in this figure legend, the reader is referred to the web version of this article.)

reduced 2016 annual GEP by $\sim 32\%$ relative to what it would have been without FTC infestation. In contrast, R_e was depressed by only 7% by the attack (measured $928 \pm 129 \text{ g C y}^{-1}$ and simulated $1003 \pm 42 \text{ g C m}^{-2} \text{ y}^{-1}$). In our analysis, FTC-infestation decreased NEP from $95 \pm 91 \text{ g C m}^{-2} \text{ y}^{-1}$ (simulated) to $-130 \pm 67 \text{ g C m}^{-2} \text{ y}^{-1}$ (measured), indicating that the stand likely would have been a C sink in 2016 without the FTC infestation. The small differences between measured and simulated E values led to the annual totals being insignificantly different (measured $332 \pm 7 \text{ mm y}^{-1}$ and simulated $339 \pm 61 \text{ mm y}^{-1}$, respectively).

4. Discussion

The impact of the FTC defoliation at OA started in early May and lasted until early July. Cook et al. (2008) also observed their stand defoliated from May to June by a single generation of FTC larvae that fed on newly emerged leaves. They observed defoliation of 37% drop in leaf area index (LAI) while we found a 83% drop in G_{CC} and 75% in ρ_s by mid-June before the refoliation of the stand. It is typical for trees to refoliate a few weeks after defoliation and for the leaves to remain smaller than leaves in years without attack (Wargo, 1981). The smaller leaves in the refoliated stand may account for the observed decrease in G_{CC} after refoliation. Although the OA stand did refoliate following the FTC attack, it did not recover to the maximum G_{CC} normally achieved at the peak of the growing season. Schäfer et al. (2010) found that after a complete defoliation event (lasting 2–3 weeks), the stand refoliated to 50% of the two previous growing seasons' foliage level. We found a much greater refoliation with our stand recovering to 96% of the average maximum G_{CC} and ρ_s reaching typical values by the end of June. A small secondary rise in G_{CC} also occurred in the second week of September 2016, just prior to canopy senescence. We note that this difference could potentially have been caused by sensor discontinuity because a new PhenoCam was in use during the end of the 2016 season and the previous camera was decommissioned and was therefore unavailable for direct comparison.

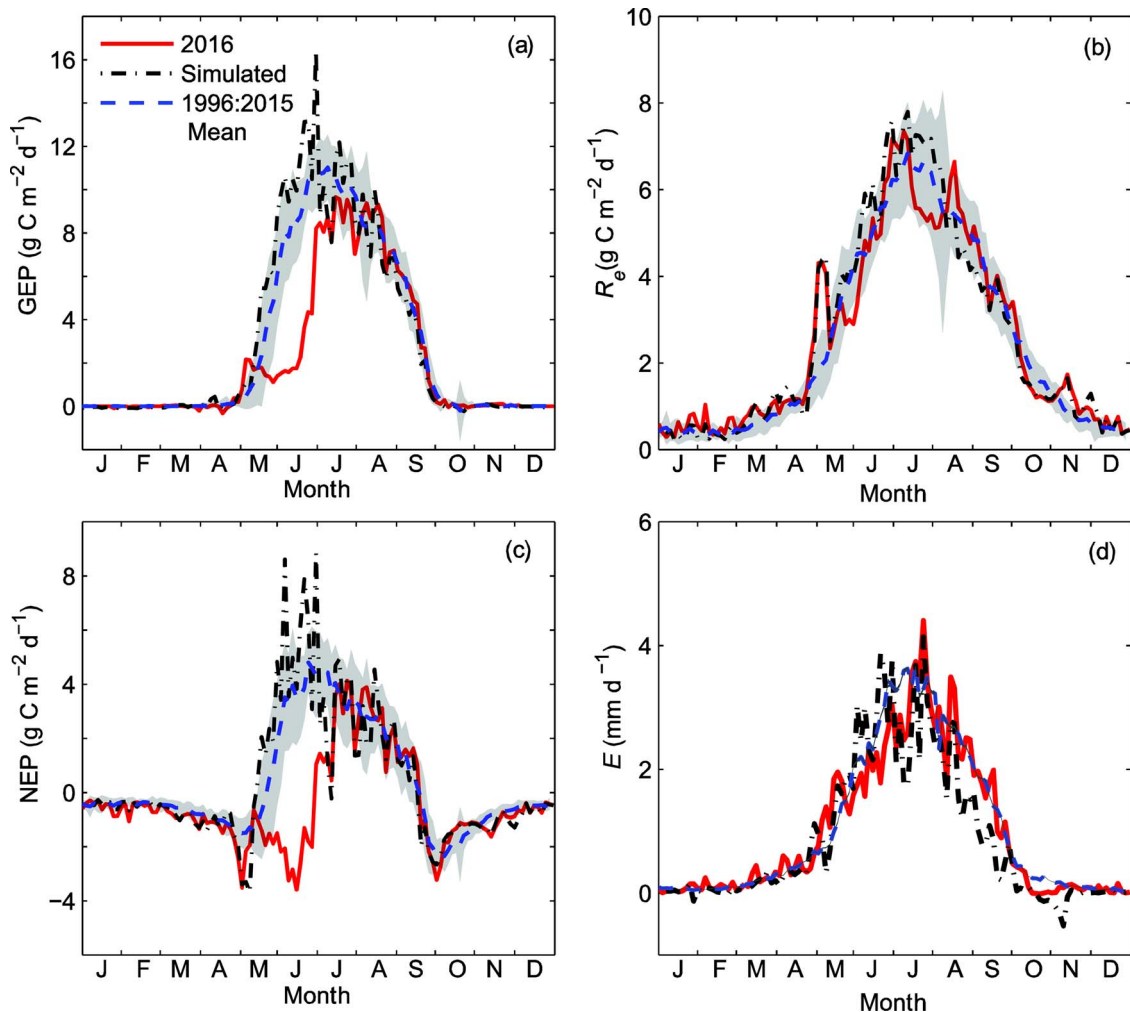


Fig. 9. Temporal progression of three-day averaged measured (red line), simulated (black dashed line), and the 1996–2015 mean (blue dashed line) for (a) gross ecosystem production (GEP), (b) ecosystem respiration (R_e), (c) net ecosystem production (NEP), and (d) evapotranspiration (E). Grey shaded areas indicate $\pm 1\sigma$ from the long-term mean. Note the shaded area for panel d is not visible because the magnitude of deviation spans a range of similar sizing to the lines. (For interpretation of the references to colour in this figure legend, the reader is referred to the web version of this article.)

The 2016 defoliation suppressed GEP by more than 75% from early May to mid-June, but the second leaf flush in June caused GEP to recover to near-normal values for the remainder of the growing season. Despite this recovery, the annual total GEP was reduced by $\sim 27\%$ compared to what it would have been without the FTC infestation. Cook et al. (2008) found that despite a re-flush of leaves following FTC defoliation, GEP remained suppressed for the rest of the growing season leading to a 24% decrease in annual GEP compared to the mean of 6 years of non-disturbed flux tower observations. We found that the reduction in measured R_e was about 30% smaller during the period from early May to early August, which resulted in an annual total that was approximately 7% lower than simulated R_e without the defoliation event. However, Cook et al. (2008) found R_e in the attack year to be about 6% greater than in the two non-attack years. Amiro et al. (2010) reported that during the year of a gypsy moth and FTC infestation in oak-pine and pitch pine-scrub oak stands, both GEP and R_e decreased. We found that the resulting NEP in 2016 was greatly decreased from early May to mid-June but was slightly higher than simulated from mid-July through August, due to simulated FTC-free R_e being much higher than measured R_e during that time. Schäfer et al. (2010) found that despite a 50% re-leafing of the stand, modelled net canopy

assimilation was reduced by 75%. In our study, annual NEP was reduced from $95 \pm 91 \text{ g C m}^{-2} \text{ y}^{-1}$ to $-130 \pm 67 \text{ g C m}^{-2} \text{ y}^{-1}$ by the defoliation event. These results that an FTC infestation switched the stand from a C sink to a C source are consistent with those observed by Hicke et al. (2012) for severe insect outbreaks.

The defoliation event caused the site to become a C source for the second time on record, but with the most negative annual NEP ever recorded at the site. The significant decrease in GEP while R_e remained slightly below the long-term mean, led to extremely low annual NEP. The year 2016 was very warm, with the highest T_a on record (1997–2016) and among the 5 warmest years in terms of T_s in the 1996–2016 observation period. Despite these warm temperatures and the early start to the growing season, the growing degree day total in 2016 was only the 4th highest on record. The early growing season start, due to warm spring temperatures, led to early foliation, which partially offset the decrease in GEP by the defoliation. The FTC-free simulation indicated that without the defoliation, annual GEP in 2016 would have been greater than the long-term mean. Surprisingly, annual R_e in 2016 was slightly lower than the long-term mean, despite the unusually warm air and soil temperatures in 2016. If the attack had not occurred, R_e would have been greater than the long-term mean.

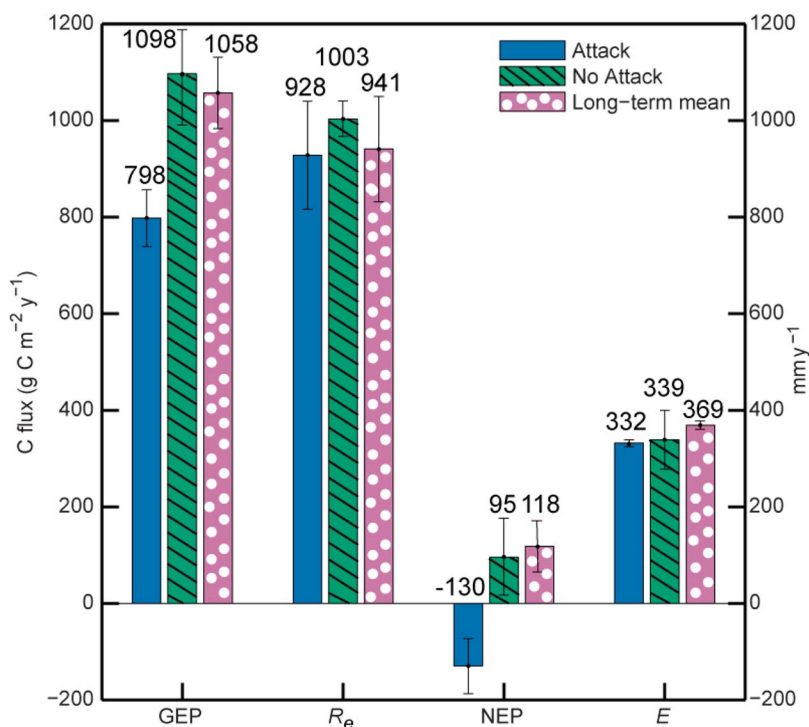


Fig. 10. Annual measured (FTC attack) in blue compared to simulated (no FTC attack) in hatched green, and the 20-year mean, in white dots on pink background, gross ecosystem production (GEP), ecosystem respiration (R_e), net ecosystem production (NEP) and evapotranspiration (E). (For interpretation of the references to colour in this figure legend, the reader is referred to the web version of this article.)

Despite the large impact on C, the FTC infestation had a minimal effect on annual E . One might hypothesize that a significant alteration to the C fluxes would also be observed in the water fluxes, but previous studies have shown why this may not be the case. Using soil moisture, radial bole growth, and xylem pressure potential measurements, Stephens et al. (1972) showed that one of the physiological impacts of a 40% defoliation event of gypsy moth on deciduous trees is reduced water loss and stress during the period when leaves are absent. Quentin et al. (2011) observed a short-term decrease in water flux after manual defoliation of eucalyptus but rates of water use in the defoliated trees were similar to the control trees when the leaf area recovered. Similar to the results of Stephens et al. (1972) and Quentin et al. (2011), after defoliation E decreased by one third to one half of simulated levels that would have occurred without the defoliation and then recovered so that they closely matched for the remainder of the year, resulting in very similar annual total E . The capability for increased transpiration by reforested stands is explained by the increased stomatal conductance to transpiration of the secondary foliage compared to the primary foliage that escaped folivory (Stephens et al., 1972), or utilization of increased soil moisture later in the growing season due to decreased E during the defoliation. A defoliation of 40% of the total plant leaf area in sugar cane increased stomatal conductance resulting in whole plant evapotranspiration and leaf water potential of the remaining leaf area being of similar magnitude to pre-defoliation levels (Meinzer and Grantz, 1990). Improved water use efficiency during defoliation and increased stomatal conductance upon reforestation are important results since it is often thought that defoliation would reduce transpiration and therefore could significantly alter stand water balances (Cunningham et al., 2009).

In eastern Alberta and western Saskatchewan several years of consecutive FTC infestations were recorded in the late 1980s (Brandt, 1995) and the defoliation during this period was associated with two major collapses in growth, observed using tree-ring analysis in Saskatchewan (Hogg and Schwarz, 1999). Hogg et al. (2002) found similar

results with tree-ring analysis in the Grande Prairie area of north-western Alberta. In 2000, the Climate Change Impacts on Productivity and Health of Aspen (CIPHA) program established forest health monitoring from northeastern British Columbia to the Northwest Territories and to southern Manitoba. During the period 1951–2000, insect defoliation was the second strongest influence on the inter-annual variation in regional-scale aspen growth, and when combined with drought produced a major collapse in aspen stands (Hogg et al., 2005, 2008). In 2012, 8.6 million hectares of forests in Canada were damaged by insects, with 3 million impacted by bark beetles and the remainder affected by spruce budworms and FTC (The State of Canada's Forests: Annual Report, 2014). Defoliators have impacted more than 100 Mha of forest in Canada and the USA combined over the past six decades (Kautz et al., 2017). The extent and impact of the combined effects of insect defoliation events and drought indicates the need of incorporating them in national- to global-scale models of forest growth and C cycling (Kurz and Apps, 1999).

With expected climate change, the capacity of forests to be C sinks is becoming even more uncertain. Forest disturbance by insects has already been shown to be impacted by human-induced climate change (Kurz et al., 2008). The majority of insect disturbances have been limited to the southern region of Canada, but with warming temperatures, expansion into areas where insects have historically not been able to thrive could lead to large alterations to the C cycle (Kurz et al., 2013). Couture et al. (2015) found that negative impacts of herbivorous insects on NEP more than doubled under elevated CO_2 concentrations, suggesting that herbivorous insects may limit the capacity of forests to be C sinks in a high CO_2 world. For every $1 \text{ g C m}^{-2} \text{y}^{-1}$ change in net C flux from Canada's boreal forest, the total change in the boreal forest C balance will be $2.7 \text{ Tg C year}^{-1}$, showing that a small change in flux over such a large area has implications for the global C cycle (Kurz et al., 2013). Since widespread outbreaks of defoliating insects are common, failure to measure such events and assess the effects on C exchange can lead to large errors in regional and continental C budgets.

5. Conclusions

- 1 During the FTC infestation period in 2016, NEP and GEP were greatly reduced, while Re was slightly reduced with all three fluxes recovering to near normal levels before the end of the growing season.
- 2 FTC infestation resulted in observed E being one half to two thirds of simulated E for a 4-week period during the defoliation period but had little effect on annual E.
- 3 FTC infestation in 2016 resulted in the most negative annual NEP ($-130 \text{ g C m}^{-2} \text{ y}^{-1}$) observed over the 1996–2016 period of flux monitoring at the OA site.
- 4 The OA stand, which has been generally a C sink since 1996, would also have been a C sink in 2016 without the FTC infestation.
- 5 Combining remote sensing indices with tower-based fluxes and indices provides verification in quantifying the intensity and extent of such a defoliation event.
- 6 Insect caused defoliation events can result in substantial but short-term impacts to water and C fluxes, with annual net C uptake decreasing more than the decrease caused by a three-year drought.

Appendix A

Acknowledgements

This research has been supported by the Fluxnet Canada Research Network (2002–2007) (NSERC, CFCAS and BIOCAP) and the Canadian Carbon Program (2008–2012) (CFCAS) and by an NSERC (Climate Change and Atmospheric Research) Grant to the Changing Cold Regions Network (CCRN) (2012–2016) and an NSERC Discovery Grant to TAB. The development of PhenoCam has been supported by the Northeastern States Research Cooperative, NSF’s Macrosystems Biology program (award EF-1065029), DOE’s Regional and Global Climate Modeling program (award DE-SC0016011), the US National Park Service Inventory and Monitoring Program, and the USA National Phenology Network (grant number G10AP00129 from the United States Geological Survey). We gratefully acknowledge the dedicated field support of Bruce Johnson and Greg Neufeld. We acknowledge the data contribution and communication of Jay Maillet. We acknowledge the coding assistance of Sung-Ching Lee. We thank Ted Hogg and Garth van der Kamp for their continued monitoring and interest at the sites.

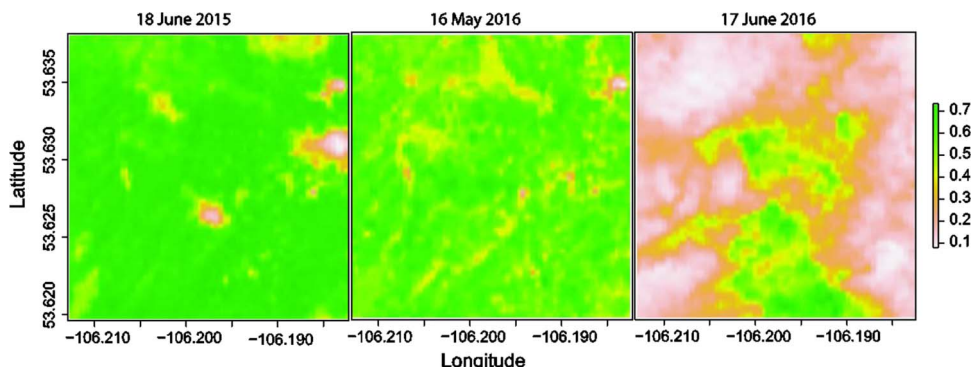


Fig. A1. NDVI data from the Landsat8 platform, which has a pixel size of 30 m × 30 m, centered on the tower and covering an area of 2 km² on 18 June 2015, 16 May 2016 and 17 June 2016.



Fig. A2. Photographs of the forest tent caterpillar (FTC) defoliation event at the Old Aspen (OA) Fluxnet site taken on 16 June 2016 from atop the tower starting north and turning in approximately 45° increments for the full 360°.

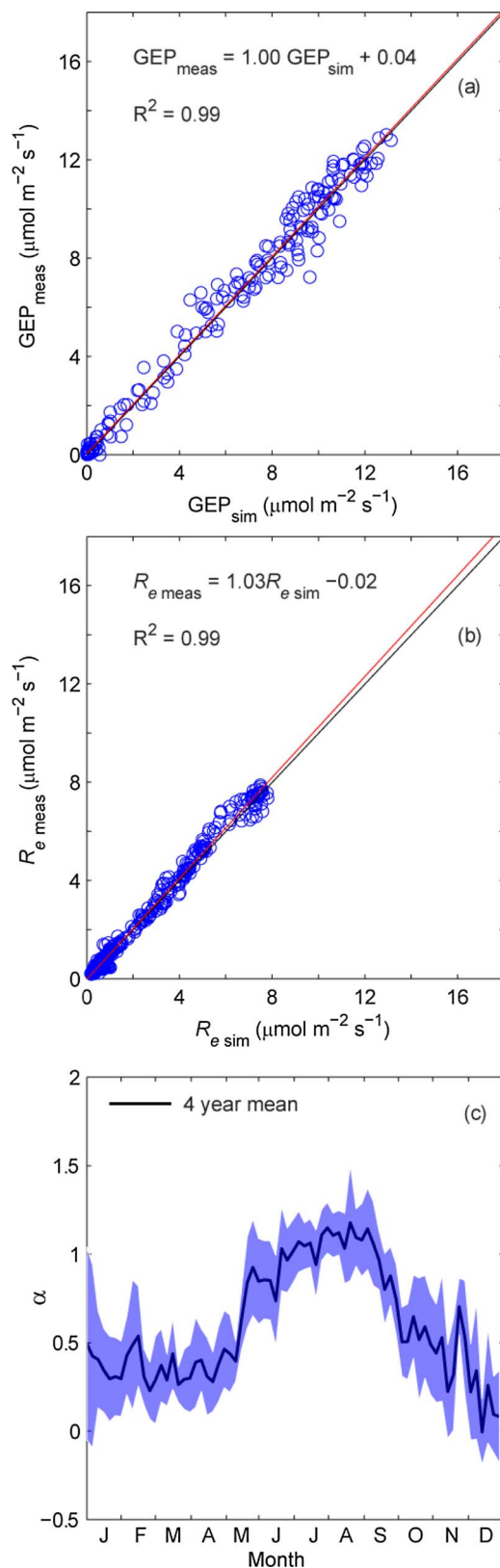


Fig. A3. Daily average measurements (average of the 4 validation years) versus simulated gross ecosystem production (GEP) (a) and ecosystem respiration (R_e) (b) ($n = 365$). Panel (c) shows five-day averaged Priestley-Taylor alpha (α) from the four years (1998, 2001, 2006, and 2010) with the standard deviation indicated by the blue shading. (For interpretation of the references to colour in this figure legend, the reader is referred to the web version of this article.)

Table A1

Fitted parameter values for Eq. (1) for R_e and Eq. (2) for GEP under low light ($PAR < 800 \mu\text{mol photons m}^{-2} \text{s}^{-1}$) and high light ($PAR > 800 \mu\text{mol photons m}^{-2} \text{s}^{-1}$) for individual years and the average of the four years.

Year	R_e			GEP			
	b_1 ($\mu\text{mol CO}_2 \text{ m}^{-2} \text{ s}^{-1}$)	b_2 ($^{\circ}\text{C}^{-1}$)	b_3 ($^{\circ}\text{C}$)	Low light		High light	
				c_1 ($\mu\text{mol CO}_2 \text{ m}^{-2} \text{ s}^{-1}$)	c_2 ($\mu\text{mol photons m}^{-2} \text{ s}^{-1}$)	c_1 ($\mu\text{mol CO}_2 \text{ m}^{-2} \text{ s}^{-1}$)	c_2 ($\mu\text{mol photons m}^{-2} \text{ s}^{-1}$)
1998	11	0.24	11	32	994	33	1072
2001	8	0.25	9	21	548	83	4685
2006	11	0.24	11	24	555	50	2155
2010	12	0.24	15	23	610	122	7464
Average	10	0.25	11	25	677	72	3844

Table A2

Summary of the comparison of simulated and measured annual values of GEP and R_e for individual years (1998, 2001, 2006, and 2010) and the 4 year average.

	GEP	R_e
Percent error	11% to – 1%	18% to – 8%
Difference ($\text{g C m}^2 \text{ y}^{-1}$)	84 to – 64 (avg. = 53)	58 to – 15 (avg. = 32)
Measurement uncertainty ($\text{g C m}^2 \text{ y}^{-1}$)	115–63 (avg. = 95)	157–98 (avg. = 134)
Slope + Intercept of 4-year average ($\text{g C m}^2 \text{ y}^{-1}$)	1.00 + 0.04	1.03 – 0.02
4-year average difference ($\text{g C m}^2 \text{ y}^{-1}$)	10	19

The results include the correction factor of 0.90 applied to the simulated R_e .

References

Amiro, B., Barr, A., Black, T., Iwashita, H., Kljun, N., McCaughey, J., Morgenstern, K., Murayama, S., Nesic, Z., Orchansky, A., 2006. Carbon, energy and water fluxes at mature and disturbed forest sites, Saskatchewan, Canada. *Agric. For. Meteorol.* 136 (3), 237–251.

Amiro, B.D., Barr, A.G., Barr, J.G., Black, T.A., Bracho, R., Brown, M., Chen, J., Clark, K.L., Davis, K.J., Desai, A.R., Dore, S., Engel, V., Fuentes, J.D., Goldstein, A.H., Goulden, M.L., Kolb, T.E., Lavigne, M.B., Law, B.E., Margolis, H.A., Martin, T., McCaughey, J.H., Misson, L., Montes-Helu, M., Noormets, A., Randerson, J.T., Starr, G., Xiao, J., 2010. Ecosystem carbon dioxide fluxes after disturbance in forests of North America. *J. Geophys. Res.: Biogeosci.* 115 (G4).

Arain, M., Black, T., Barr, A., Jarvis, P., Massheder, J., Verseghy, D., Nesic, Z., 2002. Effects of seasonal and interannual climate variability on net ecosystem productivity of boreal deciduous and conifer forests. *Can. J. For. Res.* 32 (5), 878–891.

Barr, A.G., van der Kamp, G., Black, T.A., McCaughey, J.H., Nesic, Z., 2012. Energy balance closure at the BERMS flux towers in relation to the water balance of the White Gull Creek watershed 1999–2009. *Agric. For. Meteorol.* 153, 3–13.

Barr, A.G., Black, T.A., Hogg, E.H., Griffis, T.J., Morgenstern, K., Kljun, N., Theede, A., Nesic, Z., 2007. Climatic controls on the carbon and water balances of a boreal aspen forest, 1994–2003. *Glob. Change Biol.* 13 (3), 561–576.

Barr, A.G., Black, T.A., Hogg, E.H., Kljun, N., Morgenstern, K., Nesic, Z., 2004. Inter-annual variability in the leaf area index of a boreal aspen-hazelnut forest in relation to net ecosystem production. *Agric. For. Meteorol.* 126 (3–4), 237–255.

Barr, A.G., Griffis, T.J., Black, T.A., Lee, X., Staebler, R.M., Fuentes, J.D., Chen, Z., Morgenstern, K., 2002. Comparing the carbon budgets of boreal and temperate deciduous forest stands. *Can. J. For. Res.* 32 (5), 813–822.

Brandt, J.P., 1995. Forest Insect-and Disease-Caused Impacts to Timber Resources of West-Central Canada, 1988–1992. Canadian Forest Service, Northern Forestry Centre.

Brandt, J., Cerezke, H., Mallett, K., Volney, W., Weber, J., 2003. Factors affecting trembling aspen (*Populus tremuloides* Michx.) health in the boreal forest of Alberta, Saskatchewan, and Manitoba, Canada. *For. Ecol. Manage.* 178 (3), 287–300.

Chen, B., Coops, N.C., Margolis, H.A., Amiro, B.D., Arain, M.A., Barr, A.G., Black, T.A., Bourque, C.P.-A., Flanagan, L.B., Lafleur, P.M., McCaughey, J.H., Wofsy, S.C., 2012. Characterizing spatial representativeness of flux tower eddy-covariance measurements across the Canadian Carbon Program Network using remote sensing and footprint analysis. *Remote Sens. Environ.* 124, 742–755.

Chen, B., Coops, N.C., Fu, D., Margolis, H.A., Amiro, B.D., Barr, A.G., Black, T.A., Arain, M.A., Bourque, C.P.-A., Flanagan, L.B., Lafleur, P.M., McCaughey, J.H., Wofsy, S.C., 2011. Assessing eddy-covariance flux tower location bias across the Fluxnet-Canada Research Network based on remote sensing and footprint modelling. *Agric. For. Meteorol.* 151, 87–100.

Clark, K.L., Skowronski, N., Hom, J., 2010. Invasive insects impact forest carbon

dynamics. *Glob. Change Biol.* 16 (1), 88–101.

Cook, B.D., Bolstad, P.V., Martin, J.G., Heinsch, F.A., Davis, K.J., Wang, W., Desai, A.R., Teclaw, R.M., 2008. Using light-use and production efficiency models to predict photosynthesis and net carbon exchange during forest canopy disturbance. *Ecosystems* 11 (1), 26–44.

Cooke, B.J., Lorenzetti, F., 2006. The dynamics of forest tent caterpillar outbreaks in Quebec, Canada. *For. Ecol. Manage.* 226 (1), 110–121.

Cooke, B., Lorenzetti, F., Roland, J., 2009. On the duration and distribution of forest tent caterpillar outbreaks in east-central Canada. *J. Entomol. Soc. Ont.* 140, 3–18.

Couture, J., Meehan, T., Kruger, E., Lindroth, R., 2015. Insect herbivory alters impact of atmospheric change on northern temperate forests. *Nat. Plants* 1, 15016.

Cunningham, S.A., Pullen, K.R., Colloff, M.J., 2009. Whole-tree sap flow is substantially diminished by leaf herbivory. *Oecologia* 158 (4), 633–640.

FAO, 2015. Global Forest Resources Assessment 2015: How Have the World's Forests Changed? FAO, Rome, Italy.

Griffis, T.J., Black, T.A., Morgenstern, K., Barr, A.G., Nesic, Z., Drewitt, G.B., Gaumont-Guay, D., McCaughey, J.H., 2003. Ecophysiological controls on the carbon balances of three southern boreal forests. *Agric. For. Meteorol.* 117 (1–2), 53–71.

Hicke, J.A., Allen, C.D., Desai, A.R., Dietze, M.C., Hall, R.J., Hogg, E.H., Kashian, D.M., Moore, D., Raffa, K.F., Sturrock, R.N., Vogelmann, J., 2012. Effects of biotic disturbances on forest carbon cycling in the United States and Canada. *Glob. Change Biol.* 18 (1), 7–34.

Hird, J.N., McDermid, G.J., 2009. Noise reduction of NDVI time series: an empirical comparison of selected techniques. *Remote Sens. Environ.* 113 (1), 248–258.

Hogg, E.H., Schwarz, A.G., 1999. Tree-Ring Analysis of Declining Aspen Stands in West-Central Saskatchewan. Northern Forestry Centre.

Hogg, E.H., Brandt, J.P., Kochtubajda, B., 2005. Factors affecting interannual variation in growth of western Canadian aspen forests during 1951–2000. *Can. J. For. Res.* 35 (3), 610–622.

Hogg, E.H., Brandt, J.P., Kochtubajda, B., 2002. Growth and dieback of aspen forests in northwestern Alberta, Canada, in relation to climate and insects. *Can. J. For. Res.* 32 (5), 823–832.

Hogg, E., Brandt, J., Michaelian, M., 2008. Impacts of a regional drought on the productivity, dieback, and biomass of western Canadian aspen forests. *Can. J. For. Res.* 38 (6), 1373–1384.

Hufkens, K., Friedl, M.A., Keenan, T.F., Sonnentag, O., Bailey, A., O'Keefe, J., Richardson, A.D., 2012. Ecological impacts of a widespread frost event following early spring leaf-out. *Glob. Change Biol.* 18 (7), 2365–2377.

Ives, W., Wong, H.R., 1988. Tree and Shrub Insects of the Prairie Provinces. Canadian Forestry Service, Northern Forestry Centre, Edmonton, Alberta Information Report NOR-X-292, 327 p.

Kautz, M., Meddens, A.J., Hall, R.J., Arnehan, A., 2017. Biotic disturbances in Northern Hemisphere forests—a synthesis of recent data, uncertainties and implications for forest monitoring and modelling. *Glob. Ecol. Biogeogr.* 26 (5), 533–552.

Keenan, T.F., Darby, B., Felts, E., Sonnentag, O., Friedl, M.A., Hufkens, K., O'Keefe, J.,

- Klosterman, S., Munger, J.W., Toomey, M., Richardson, A.D., 2014. Tracking forest phenology and seasonal physiology using digital repeat photography: a critical assessment. *Ecol. Appl.* 24 (6), 1478–1489.
- Kljun, N., Black, T.A., Griffis, T.J., Barr, A.G., Gaumont-Guay, D., Morgenstern, K., McCaughey, J.H., Nescic, Z., 2006. Response of net ecosystem productivity of three boreal forest stands to drought. *Ecosystems* 9 (7), 1128–1144.
- Krishnan, P., Black, T.A., Grant, N.J., Barr, A.G., Hogg, E.H., Jassal, R.S., Morgenstern, K., 2006. Impact of changing soil moisture distribution on net ecosystem productivity of a boreal aspen forest during and following drought. *Agric. For. Meteorol.* 139 (3–4), 208–223.
- Kurz, W.A., Apps, M.J., 1999. A 70-year retrospective analysis of carbon fluxes in the Canadian forest sector. *Ecol. Appl.* 9 (2), 526–547.
- Kurz, W.A., Shaw, C., Boisvenue, C., Stinson, G., Metsaranta, J., Leckie, D., Dyk, A., Smyth, C., Neilson, E., 2013. Carbon in Canada's boreal forest—a synthesis 1. *Environ. Rev.* 21 (4), 260–292.
- Kurz, W.A., Stinson, G., Rampley, G.J., Dymond, C.C., Neilson, E.T., 2008. Risk of natural disturbances makes future contribution of Canada's forests to the global carbon cycle highly uncertain. *Proc. Natl. Acad. Sci. U. S. A.* 105 (5), 1551–1555.
- Lange, M., Doktor, D., 2017. **Phenex: Auxiliary Functions for Phenological Data Analysis. R Package Version 1.4–5.** <https://CRAN.R-project.org/package=phenex>.
- Man, R., Rice, J.A., 2010. Response of aspen stands to forest tent caterpillar defoliation and subsequent overstory mortality in northeastern Ontario, Canada. *For. Ecol. Manage.* 260 (10), 1853–1860.
- Meinzer, F., Grantz, D., 1990. Stomatal and hydraulic conductance in growing sugarcane: stomatal adjustment to water transport capacity. *Plant Cell Environ.* 13 (4), 383–388.
- Morgenstern, K., Black, T.A., Humphreys, E.R., Griffis, T.J., Drewitt, G.B., Cai, T., Nescic, Z., Spittlehouse, D.L., Livingston, N.J., 2004. Sensitivity and uncertainty of the carbon balance of a Pacific Northwest Douglas-fir forest during an El Niño/La Niña cycle. *Agric. Forest Meteorol.* 123 (3), 201–219.
- Natural Resources Canada “The State of Canada's Forests: Annual Report, 2014. Cat. No. Fo1-6/2014E-PDF ISSN 1488-2736 <https://cfs.nrcan.gc.ca/series/read/90>.
- Peterson, E., Peterson, N., 1992. Ecology, management, and use of aspen and balsam poplar in the prairie provinces. *Spec. Rep.* 1, 252.
- Priestley, C., Taylor, R., 1972. On the assessment of surface heat flux and evaporation using large-scale parameters. *Mon. Weather Rev.* 100 (2), 81–92.
- Quentin, A.G., O'Grady, A.P., Beadle, C.L., Worledge, D., Pinkard, E.A., 2011. Responses of transpiration and canopy conductance to partial defoliation of *Eucalyptus globulus* trees. *Agric. For. Meteorol.* 151 (3), 356–364.
- R Core Team, 2017. **R: A Language and Environment for Statistical Computing.** URL: <https://www.R-project.org/>.
- Reifsnyder, W.E., 1967. Radiation geometry in the measurement and interpretation of radiation balance. *Agric. Meteorol.* 4 (4), 255–265.
- Richardson, A.D., Braswell, B.H., Hollinger, D.Y., Jenkins, J.P., Ollinger, S.V., 2009. Near-surface remote sensing of spatial and temporal variation in canopy phenology. *Ecol. Appl.* 19 (6), 1417–1428.
- Richardson, A.D., Jenkins, J.P., Braswell, B.H., Hollinger, D.Y., Ollinger, S.V., Smith, M., 2007. Use of digital webcam images to track spring green-up in a deciduous broadleaf forest. *Oecologia* 152 (2), 323–334.
- Schäfer, K.V., Clark, K.L., Skowronski, N., Hamerlynck, E.P., 2010. Impact of insect defoliation on forest carbon balance as assessed with a canopy assimilation model. *Glob. Change Biol.* 16 (2), 546–560.
- Sonnentag, O., Hufkens, K., Teshera-Sterne, C., Young, A.M., Friedl, M., Braswell, B.H., Milliman, T., O'Keefe, J., Richardson, A.D., 2012. Digital repeat photography for phenological research in forest ecosystems. *Agric. For. Meteorol.* 152, 159–177.
- Stephens, G.R., Turner, N.C., De Roo, H.C., 1972. Notes: some effects of defoliation by gypsy moth (*Porthetria dispar* L.) and Elm spanworm (*Ennomos subsignarius* Hbn.) on water balance and growth of deciduous forest trees. *For. Sci.* 18 (4), 326–330.
- Stocker, T., Qin, D., Plattner, G., Tignor, M., Allen, S., Boschung, J., Nauels, A., Xia, Y., Bex, B., Midgley, B., 2013. IPCC, 2013: Climate Change 2013: the Physical Science Basis. Contribution of Working Group I to the Fifth Assessment Report of the Intergovernmental Panel on Climate Change.
- Toomey, M., Friedl, M.A., Frolking, S., Hufkens, K., Klosterman, S., Sonnentag, O., Baldocchi, D.D., Bernacchi, C.J., Biraud, S.C., Bohrer, G., 2015. Greenness indices from digital cameras predict the timing and seasonal dynamics of canopy-scale photosynthesis. *Ecol. Appl.* 25 (1), 99–115.
- Vermote, E., Roger, J., Ray, J., 2015. MODIS Surface Reflectance User'S Guide [R/OL]. MODIS Land Surface Reflectance Science Computing Facility.
- Volney, W.J.A., Fleming, R.A., 2000. Climate change and impacts of boreal forest insects. *Agric. Ecosyst. Environ.* 82 (1), 283–294.
- Wargo, P.M., 1981. Defoliation and Tree Growth. The Gypsy Moth: Research Toward Integrated Pest Management 1584. USDA Forest Service, Science and Education Agency, Tech Bull, pp. 225–240.
- Webb, E.K., Pearman, G.I., Leuning, R., 1980. Correction of flux measurements for density effects due to heat and water vapour transfer. *Q. J. R. Meteorol. Soc.* 106 (447), 85–100.
- Zha, T., Barr, A.G., van der Kamp, G., Black, T.A., McCaughey, J.H., Flanagan, L.B., 2010. Interannual variation of evapotranspiration from forest and grassland ecosystems in western Canada in relation to drought. *Agric. Forest Meteorol.* 150 (11), 1476–1484.